Sensitivity of internal tide generation in Hawaii

B. S. Powell,[1] I. Janeković,[1,2] G. S. Carter,[1] and M. A. Merrifield[1]

Received 19 March 2012; revised 26 April 2012; accepted 27 April 2012; published 24 May 2012.

[1] Energy from the barotropic tide is transferred into the baroclinic tide over topographic gradients, which provides a mechanism for the ocean boundaries to communicate with the deep ocean, to close energy budgets, and as a source of flux affecting nutrient supply and larval transport. Understanding the temporal variability of the conversion from barotropic to baroclinic tides is critical to our understanding of these processes. Using a numerical model and its adjoint, we examine the sensitivity of tidal conversion at Kaena Ridge in Hawaii. We find a sensitivity to changes in the upper ocean due to a phase difference between the pressure anomaly and tidal velocity caused by internal waves generated on the opposite slope of the ridge; however, we also find that conversion is equally as sensitive to local, deep stratification changes. **Citation:** Powell, B. S., I. Janeković, G. S. Carter, and M. A. Merrifield (2012), Sensitivity of internal tide generation in Hawaii, *Geophys. Res. Lett.*, *39*, L10606, doi:10.1029/2012GL051724.

1. Introduction

[2] Tidally induced internal waves are responsible for balancing the deep ocean energy budget by helping to maintain stratification [*Munk*, 1966] and are capable of mass transport into the interior [*Armi*, 1978] that may impact the ecology of the oligotrophic ocean. The Hawaiian archipelago is a significant site of barotropic to baroclinic tidal conversion [*Dushaw et al.*, 1995; *Ray and Mitchum*, 1996, 1997; *Rainville et al.*, 2010] with the majority of the energy in the main islands converted at Kaena Ridge [*Merrifield and Holloway*, 2002; *Simmons et al.*, 2004; *Carter et al.*, 2008]. Using a numerical model, *Carter et al.* [2008] determined that 85% of the 2.7 GW of M_2 energy removed from the barotropic tide at Kaena Ridge is converted directly into the baroclinic tide. Kaena Ridge is an excellent laboratory to examine the conversion of energy from the barotropic to baroclinic as was shown in the Hawaii Ocean Mixing Experiment (HOME) [*Rudnick et al.*, 2003; *Pinkel and Rudnick*, 2006]: an intensive project to examine the diapycnal vertical mixing around Hawaii that resulted from the strong internal tides.

[3] What is less well known is the effect that the changing ocean stratification (by remote internal waves, the sub- and meso-scale, and low-frequency dynamics) has in determining the conversion and propagation of internal tides. Prior research [e.g., *Dushaw*, 2002] suggests that the baroclinic tides are mostly coherent with little time-variation, while recent papers [*Martini et al.*, 2007; *Kelly and Nash*, 2010; *Inall et al.*, 2011] examine the incoherence of the baroclinic tides. *Zilberman et al.* [2011] recently examined a time-series of mooring observations south of the ridge along with global circulation models to provide a description of how the ocean circulation affected the barotropic conversion. It was found that the rate of conversion varied by a factor of two over the observed period, and it was surmised that the primary reason for this variability was due to phase lag changes between the pressure anomaly and the barotropic vertical velocity from passing internal waves generated on the northern ridge. Understanding of the baroclinic tides is crucial to developing an oceanic energy budget, and the conversion of the barotropic to baroclinic is one necessary step. This work examines the variability of the conversion that would lead to incoherent baroclinic tides by using an adjoint model to examine the sensitivity of the tidal conversion to the underlying ocean circulation.

2. Model

[4] We used the Regional Ocean Modeling System (ROMS): a free-surface, hydrostatic, primitive equation model discretized with a terrain following vertical coordinate system [*Shchepetkin and McWilliams*, 2005]. ROMS has been widely applied in many applications (see http://www.myroms.org for a list of published ROMS papers). It is a hydrostatic model, which can affect the generation of internal waves; however, as shown in *Bergh and Berntsen* [2008], for the resolution and significant strength of internal waves we are interested in, the non-hydrostatic component is negligible. The model was configured with a four-kilometer horizontal resolution model using 30 levels of vertical, terrain-following coordinates for the Hawaiian region with *Mellor and Yamada* [1982] level-2.5 vertical turbulence closure. This mixing scheme has been shown to well-represent the generation of internal tides [*Robertson*, 2006]. The model was integrated for calendar year 2010 using lateral boundary conditions prescribed from the Navy Coastal Ocean Model (NCOM) [*Barron et al.*, 2006]. Surface forcing was provided by a locally produced high-resolution Weather Regional Forecast (WRF) model. The model was integrated using 11 barotropic tidal constituents generated from the global tidal solution provided by the Oregon State University TOPEX/Poseidon Global Inverse Solution (TPXO) [*Egbert and Erofeeva*, 2002]. We use a full-range of constituents to better capture the interaction between the major tidal constituents and their role in the barotropic to baroclinic conversion.

[5] In s-level models, sharp changes in bathymetry may result in significantly large (>0.25) *r*-factor values (ratio of the difference between the total height and heights of two

[1]Department of Oceanography, University of Hawaii at Manoa, Honolulu, Hawaii, USA.
[2]On leave from Institute Rudjer Boskovic, Zagreb, Croatia.

Corresponding author: B. S. Powell, Department of Oceanography, University of Hawaii at Manoa, 1000 Pope Rd., MSB, Honolulu, HI 96822, USA. (powellb@hawaii.edu)

0094-8276/12/2012GL051724

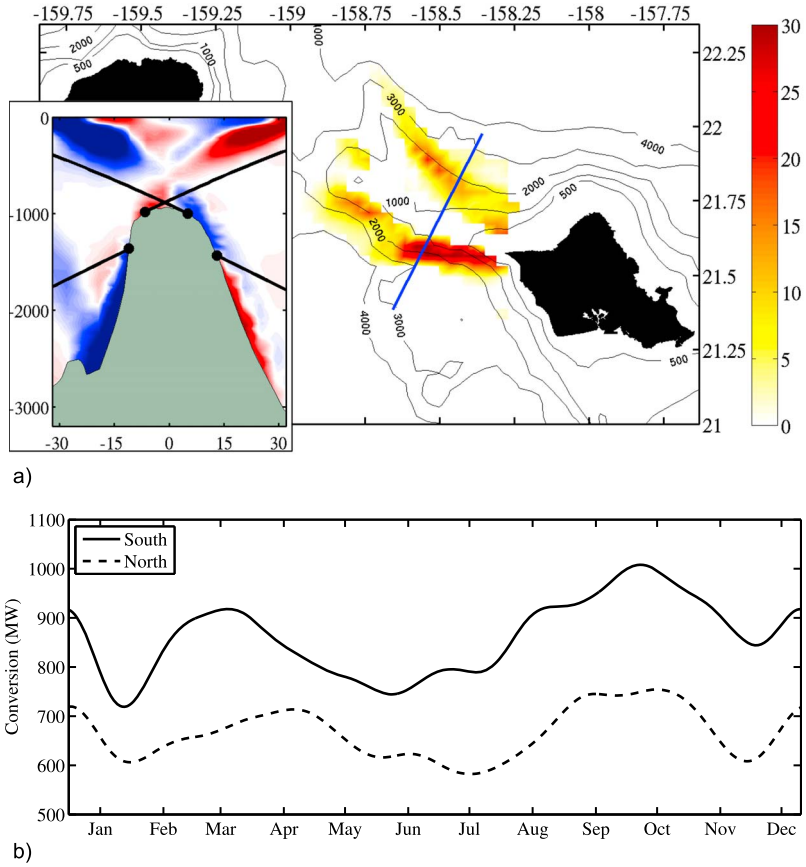

Figure 1. (a) Map of Kaena ridge with mean conversion in MW (inset) semi-diurnal flux along the blue transect line where red (blue) flux is to the northeast (southwest) and the theoretical ray paths for typical stratification are shown for four conversion sites. (b) Time-series of total tidal conversion for the modeled period.

adjacent cells) that create horizontal pressure gradient errors. ROMS is effective at minimizing these errors [*Shchepetkin and McWilliams*, 2003]; however, special consideration must be applied to the bathymetric representation. Complicating the situation, steep topography is required to capture the full energy conversion of the barotropic-to-baroclinic tidal exchange [*Di Lorenzo et al.*, 2006]; however, we are interested only in the sensitivity of the total conversion to perturbations rather than the absolute total conversion itself.

[6] Conversion from the barotropic to baroclinic tides is computed in the same way as *Nash et al.* [2005] by

$$C_i = \left\langle \left[p(-H_i) - \bar{p}(-H_i) - p_i^s\right](\bar{u}_i)_\theta \cdot \nabla(-H_i) \right\rangle_\theta, \qquad (1)$$

where $\langle \cdot \rangle$ is the arithmetic mean, i is a grid location of the model, $p(-H_i)$ is the pressure at the bottom, $\bar{p}(-H_i)$ is the temporal mean of bottom pressure, $\bar{u}_\theta$ is the barotropic tidal velocity for period θ, $\nabla(-H)$ is the bathymetric slope $(u_i)_\theta \cdot \nabla(-H_i)$ is therefore the barotropic tidal vertical velocity, w_{bt}), and p_i^s is the baroclinic surface pressure correction given by $p_i^s = \frac{1}{H_i}\int_{-H_i}^{0} (p(z_i) - \bar{p}(z_i))\, dz$. Equation (1) provides the energy conversion rate in W m^{-2}. There is little seasonality in the stratification around Kaena ridge, so $\bar{p}$ is taken from the full integration period. We consider only the conversion due to the major semidiurnal tides (M_2, S_2, N_2, and K_2), and we use an averaging period of 25 hours (two full cycles) to compute the conversion. To determine the total amount of energy converted along the ridge, all considered points are scaled by the bottom area and summed. For this work, we focus on model grid points along both flanks of the ridge ranging in depth from 4000 m to 340 m (see Figure 1).

2.1. Adjoint Method

[7] To quantify the effects of the ocean dynamics on the conversion, we use the adjoint model of ROMS (ADROMS) as defined in *Moore et al.* [2004]. Derivations of the adjoint model are well documented in *Errico* [1997], *Marotzke et al.* [1999], and *Moore et al.* [2004]. Briefly, ADROMS is the adjoint of the linearized primitive equations, which—by definition—solves the Jacobian of the system. This information quantifies how some measure of the ocean varies with changes to the ocean state itself. The ROMS adjoint model has been used to study the circulation sensitivities along both the California [*Chhak and Di Lorenzo*, 2007; *Veneziani et al.*, 2009; *Moore et al.*, 2009] and New Jersey [*Zhang et al.*, 2009] coasts.

[8] We define the state of the ocean determined by the forward integration of the ROMS model as $\mathbf{x}(t)$ that contains all state variables (free surface, velocity, temperature, salt, boundary conditions, and surface forcing) of the model at all grid points for a given time, t. We further define a scalar functional, $\mathcal{J} = G(\mathbf{x}(t))$, where G is an arbitrary function that acts upon the ocean state and $\mathcal{J}$ is a scalar value. For this

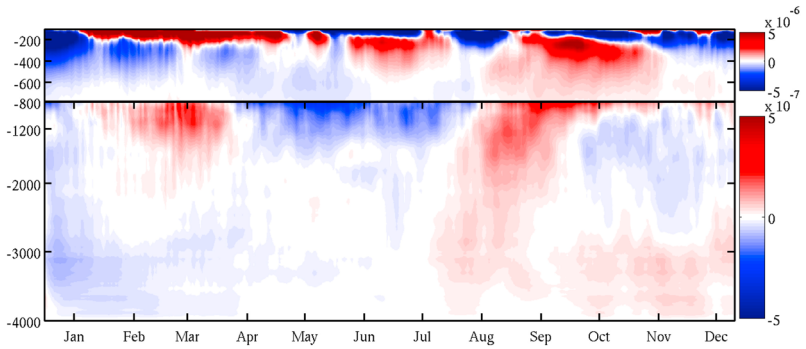

Figure 2. Spatial mean N^2 anomalies around the ridge for the year (s^{-2}). Note the differing color scales for the upper 800 m with an order of magnitude reduction.

work, we are interested in the total barotropic to baroclinic conversion and $\mathcal{J}$ is given by the total conversion from every point, i, on the ridge multiplied by the bottom area (A_i),

$$\mathcal{J} = \sum_{i=1}^{M} A_i C_i, \tag{2}$$

where C_i is given by (1) and M are the number of points considered.

[9] The adjoint model linearizes about a trajectory generated by the forward integration. The validity of this linearization is limited in time as nonlinear effects diverge from the linearization. As shown in *Matthews et al.* [2012] four days is the limit of linearity for the resolution and dynamics present in this model configuration. Therefore, for each 96 hour period over one year, we will examine how the conversion over the final 25 hours was sensitive to changes in the ocean state during the 96 hour period. By forcing the adjoint model with the derivatives of $\mathcal{J}$ with respect to the model state over the final 25 hours, the adjoint will provide the sensitivity of the conversion to the entire model state over the four days of interest. As the hydrostatic form of (1) depends only upon temperature, salinity, u, and v, we force the adjoint model with: $\partial\mathcal{J}/\partial\mathbf{T}$, $\partial\mathcal{J}/\partial\mathbf{S}$, $\partial\mathcal{J}/\partial\mathbf{u}$, and $\partial\mathcal{J}/\partial\mathbf{v}$ at each conversion point over the final 25 hours. The derivatives are computed using the forward integration for each 96 hour time period of interest. We can then determine how a single 25 hour conversion period of barotropic to baroclinic tides is sensitive to changes in the ocean state over a four day period.

3. Results and Discussion

[10] The conversion from each side of the ridge is shown in Figure 1b with the beat frequencies due to the combination of the semi-diurnal tides removed via a 42 day cutoff (the ~200 day $K_2 - S_2$ beat remains). The time-mean total conversion is found to be 1.53 GW, which is 33% lower than the M_2 conversion found by *Carter et al.* [2008] and consistent with the similar resolution model results of *Merrifield and Holloway* [2002]. The variability of the filtered conversion is 120 MW due to long-term changes in the stratification; however, during spring (neap) tide, the conversion is over 3 GW (below 200 MW). The distribution of the conversion along the northern and southern ridges is 44% and 56%, respectively (similar to *Carter et al.* [2008]).

[11] During the simulated year, two cyclonic eddies of differing strengths affected the ridge. Over the March period, a smaller eddy with a core depth less than 400 m passed well south of the ridge; however, its signature was seen in the temperature anomalies that dominate the buoyancy frequency anomalies as shown in Figure 2. A minor increase in eddy kinetic energy over the ridge was found related to this eddy. More significantly, during the warm summer period (the seasonal summer warming in Hawaii peaks in Sept.), a large cyclonic eddy passed very close to the ridge with a temperature signature below 400 m and at the eddy margins increased the temperature along the ridge. Because these temperature anomalies were increased during the peak seasonal temperatures, the warmer anomalies persisted beyond the time period that the eddy was in the region (late July–early Sept.). The eddy kinetic energy during this period increased by a factor of three. As shown in Figure 1, the conversion—particularly along the southern ridge—increased during both positive temperature anomaly periods.

[12] Temperature is the driving factor in the buoyancy frequency anomalies below 800 m; however, in the upper 800 m, temperature does not control N^2 as strongly. Below 800 m, the buoyancy frequency increases or decreases with similar variations to temperature. Of particular interest are these deep N^2 anomalies found in the model. These same types of deep anomalies were observed during HOME [*Zilberman et al.*, 2011], and they may be a signature of long Rossby waves that are communicated into the model by the global NCOM solution. These long-period fluctuations in conversion are interesting; however, on shorter time-scales, there is a difference between local changes to the pressure generating conversion force and to changes in p' phase due to remotely generated internal waves. It should be noted that in this model simulation, the only remotely generated internal tides are from the opposite sides of the ridge as Mode-1 waves from distant sources (e.g., Aleutians) are not included.

3.1. Sensitivities

[13] The results of the adjoint integration provide the sensitivity of $\mathcal{J}$ as defined in equation (2) with respect to the model and forcing fields. To better understand the results, we create an analysis metric, $\Delta\mathcal{J}_i = \left(\frac{\partial\mathcal{J}_i}{\partial x_i}\right)\sigma_{x_i}$, where i is the

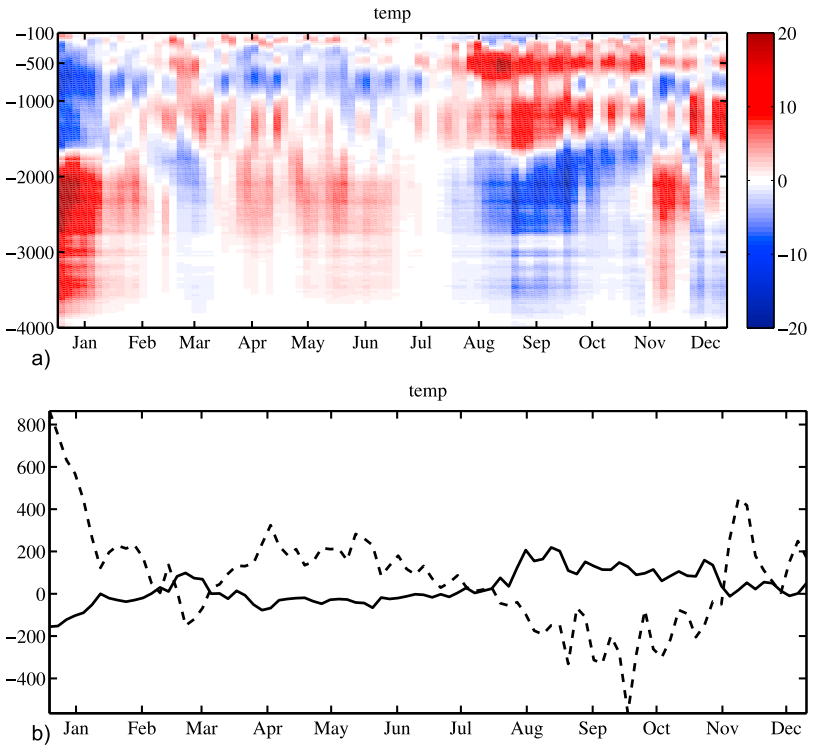

Figure 3. (a) Depth and time-variations of the total sensitivity of conversion ($\Delta\mathcal{J}$) to standard deviation changes in temperature with units in MW. (b) Integration of $\Delta\mathcal{J}$ from 100–700 m depth(downward phase propagation) in solid line and deeper than 800 m (upward phase propagation) in dashed line.

point of interest (in space and time), x is the field of interest, $\partial\mathcal{J}/\partial x$ is the output of the adjoint model, and σ_x is the standard deviation. $\Delta\mathcal{J}$ provides a measure of the change in $\mathcal{J}$ due to a single standard deviation change in variable x at location i. The σ_x values are taken from a long-term model integration without tides, such that the non-tidal variability of the ocean at each grid cell is used to normalize the sensitivities. Thus, $\Delta\mathcal{J}$ = 1 MW tells us that if that point were positively perturbed by one σ_x over the four day period, the total conversion would be changed by 1 MW. Negative values indicate where the perturbation results in a decrease in the energy converted.

[14] We first examine the spatial sum of the four day temporal mean $\Delta\mathcal{J}$ values from points along the northern and southern ridges to understand the sensitivity of the conversion to vertical stratification of temperature. Figure 3a shows the time-series of the total $\Delta\mathcal{J}$ over all conversion points for all depths. We note that there are three distinct layers: 100–750 m, 800–1800 m, and deeper than 1800 m. *Nash et al.* [2006] observed that on the south side of the ridge, the upward propagating wave energy (downward propagating phase) was confined in the upper 700 m, and below, the energy propagated downward (upward propagating phase). The model exhibits similar structure as shown by the inset of Figure 1a. Along the ridge-slope (where conversion occurs), the energy flux of the upper 750 m originates from the opposite side. Other than at the ridge top, local flux tends downward as evidenced by the theoretical ray paths calculated from the mean stratification. A small canyon exists along the southern slope, which creates additional upward energy flux, but it does not reach the upper 750 m over conversion points considered. The model well represents both the structure observed by *Nash et al.* [2006] and the results of *Carter et al.* [2006]. As shown by (1), the conversion is sensitive to the phasing between p' and w_{bt}. If we assume that over four days, the semidiurnal w_{bt} is invariant, we may assume the sensitivities in Figure 3a are due to variations of p'.

[15] The polarity of $\Delta\mathcal{J}$ between the upper layer (750 m and shallower) is often opposite of the layers below, which is indicative of the phase propagation. The processes responsible for this phasing of p' are different between the upper and lower layers. The pressure anomaly in the lower portion of the water column is dependent primarily upon local stratification anomalies (advected waters, etc.); therefore, when a local conversion cycle is larger than its mean, it is most sensitive to negative density anomalies in the lower portion of the water column that would restore the system to the mean state. In the upper ocean, the phasing of p' is affected by propagating internal waves from the opposite side of the ridge. We ascribe the layered sensitivity and this polarity to the local and remote effects that are altering the conversion (remote effects are noted in *Zilberman et al.* [2009], *Kelly and Nash* [2010], and *Hall and Carter* [2011]).

[16] During the eddy periods (March and August), the temporal polarity of the sensitivity changed along with the temperature anomaly polarity. Along with each eddy period, there is a positive N^2 anomaly and an increase in the conversion. For the deep layer, away from phase-lag changes, there is — in essence — a preferred conversion around the mean stratification and deviations from this mean alter the sensitivity of the conversion. When the temperature is already warm, increasing the temperature further in the upper ocean increases the conversion. In the deeper ocean,

when the stratification is less stable (positive N^2 anomalies), decreasing the temperature will lead to greater conversion; whereas, the same for increasing the temperature during more stable periods.

[17] Of particular importance is whether the remote phasing effects or local density anomalies have a greater impact upon the conversion. Integrating $\Delta\mathcal{J}$ over the upper 100 to 750 m provides an estimate of the total change in conversion if the upper layer changed by a single standard deviation over the four-day period. Figure 3b shows that generally the sensitivity in the upper regions where phase changes impact the conversion is relatively weak, averaging around 37 MW (during negative N^2 anomalies). During the positive N^2 anomaly periods, the sensitivity averages 97 MW, peaking at 200 MW sensitivity to changes in temperature. Conversely, for the downward energy flux region (below 800 m), the sensitivities are much greater, averaging 187 MW in standard conditions, but decrease to 158 MW during positive N^2 conditions. Comparing to Figure 1, which shows the conversion generated by the forward model during these periods, we see increases of up to 200 MW of conversion during the positive N^2 anomalies.

[18] Although we have focussed the discussion on the sensitivity to temperature changes, the adjoint provides the sensitivity relative to all model fields and forcing. The temperature dominates the conversion sensitivity. For the upper ocean, we find that $\Sigma\Delta\mathcal{J}$ is as large as 200 MW from temperature variations, but only 50 MW from variability in salt. Unsurprising, the conversion is insensitive to variability in the wind stress curl, with $\Sigma\Delta\mathcal{J} = 50KW$. Free-surface variability affects the pressure, and the sensitivity magnitude is similar to salt with $\Sigma\Delta\mathcal{J} = 50\ MW$. Of particular interest is the sensitivity to the cross- and along-ridge velocities. Focussing on the upper region, the sensitivity to cross-ridge velocity $\Sigma\Delta\mathcal{J}$ is nearly 50 MW; however, the along-ridge velocity sensitivity is 100 MW, second only to temperature perturbations. The remote internal waves propagate cross-shelf in the upper 700 m; however, it is the deep along-ridge advective flow that impacts the local conversion and may be driving the deep N^2 anomalies.

4. Consequences

[19] The adjoint model is a powerful tool that can be used for many geophysical problems to understand the dynamic variability. Using the adjoint, we have found that the local tide conversion is similarly sensitive to local stratification changes as it is to temporal variability in the phase-lag between the pressure perturbations and the tidal velocity. These phase-lag changes are due to remotely generated internal waves that propagate over the top of the ridge in the upper 750 m. Changes in conversion were most sensitive to stratification variability due to temperature and were less sensitive to salinity (due to salinity being more temporally stable). Both the model and HOME data [*Zilberman et al.*, 2011] exhibit an incoherence in the tidal conversion; however, satellite studies find largely coherent internal tides around Hawaii [*Ray and Mitchum*, 1996, 1997]. Because the satellites are most effective at sampling Mode-1 internal waves, much of the incoherence may be found in higher mode waves. Understanding the cause of temporal incoherence in the baroclinic tides is crucial to closing the regional energy budget. We agree with *Kelly and Nash* [2010] that global models with proper resolution are needed to help resolve local conversion because the conversion is sensitive to remote effects. It is important to quantify the sensitivity of the conversion because the baroclinic tides are a relentless source of mixing for momentum, sediment, nutrients, and other ecological parameters into the deep ocean.

[20] **Acknowledgments.** We thank the two anonymous reviewers for their contributions to the manuscript. B. S. Powell was supported by The Office of Naval Research grant N00014-09-10939 and I. Janeković was supported on NOAA grant NA10NOS4730016. G. S. Carter was supported by NSF grant OCN0825266. M. A. Merrifield was support by NOAA grant NA09OAR4320075. We thank Yi-Leng Chen from the Dept. of Meteorology at the University of Hawaii for providing the WRF output. This is SOEST Publication #8666.

[21] The Editor thanks two anonymous reviewers for assisting with the evaluation of this paper.

References

Armi, L. (1978), Some evidence for boundary mixing in the deep ocean, *J. Geophys. Res.*, *83*, 1971–1979.

Barron, C. N., C. A. Kara, P. J. Martin, R. C. Rhodes, and L. F. Smedstad (2006), Formulation, implementation and examination of vertical coordinate choices in the Global Navy Coastal Ocean Model (NCOM), *Ocean Modell.*, *11*, 347–375.

Bergh, J., and J. Berntsen (2008), Numerical studies of wind forced internal waves with a nonhydrostatic model, *Ocean Dyn.*, *59*, 1025–1041.

Carter, G. S., M. C. Gregg, and M. A. Merrifield (2006), Flow and mixing around a small seamount on Kaena Ridge, Hawaii, *J. Phys. Oceanogr.*, *36*, 1036–1052.

Carter, G. S., M. A. Merrifield, J. M. Becker, K. Katsumata, M. C. Gregg, D. S. Luther, M. D. Levine, T. J. Boyd, and Y. L. Firing (2008), Energetics of M_2 barotropic-to-baroclinic tidal conversion at the Hawaiian Islands, *J. Phys. Oceanogr.*, *38*, 2205–2223.

Chhak, K., and E. Di Lorenzo (2007), Decadal variations in the California Current upwelling cells, *Geophys. Res. Lett.*, *34*, L14604, doi:10.1029/2007GL030203.

Di Lorenzo, E., W. R. Young, and S. Llewellyn Smith (2006), Numerical and analytical estimates of M_2 tidal conversion at steep oceanic ridges, *J. Phys. Oceanogr.*, *36*, 1072–1084.

Dushaw, B. D. (2002), Mapping low-mode internal tides near Hawaii using TOPEX/POSEIDON altimeter data, *Geophys. Res. Lett.*, *29*(8), 1250, doi:10.1029/2001GL013944.

Dushaw, B. D., B. M. Howe, B. D. Cornuelle, P. F. Worcester, and D. S. Luther (1995), Barotropic and baroclinic tides in the central North Pacific Ocean determined from long-range reciprocal acoustic transmissions, *J. Phys. Oceanogr.*, *25*, 631–647.

Egbert, G. D., and S. Y. Erofeeva (2002), Efficient inverse modeling of barotropic ocean tides, *J. Atmos. Oceanic Technol.*, *19*, 183–204.

Errico, R. M. (1997), What is an adjoint model?, *Bull. Am. Meteorol. Soc.*, *78*, 2577–2591.

Hall, R. A., and G. S. Carter (2011), Internal tides in Monterey Submarine Canyon, *J. Phys. Oceanogr.*, *41*, 186–204.

Inall, M., D. Aleynik, T. Boyd, M. Palmer, and J. Sharples (2011), Internal tide coherence and decay over a wide shelf sea, *Geophys. Res. Lett.*, *38*, L23607, doi:10.1029/2011GL049943.

Kelly, S. M., and J. D. Nash (2010), Internal-tide generation and destruction by shoaling internal tides, *Geophys. Res. Lett.*, *37*, L23611, doi:10.1029/2010GL045598.

Marotzke, J., R. Giering, K. Q. Zhang, D. Stammer, C. Hill, and T. Lee (1999), Construction of the adjoint MIT ocean general circulation model and application to Atlantic heat transport sensitivity, *J. Geophys. Res.*, *104*, 29,529–29,547.

Martini, K. I., M. H. Alford, J. D. Nash, E. Kunze, and M. A. Merrifield (2007), Diagnosing a partly standing internal wave in Mamala Bay, Oahu, *Geophys. Res. Lett.*, *34*, L17604, doi:10.1029/2007GL029749.

Matthews, D., B. S. Powell, and I. Janeković (2012), Analysis of four-dimensional variational state estimation of the Hawaiian waters, *J. Geophys. Res.*, *117*, C03013, doi:10.1029/2011JC007575.

Mellor, G. L., and T. Yamada (1982), Development of a turbulence closure model for geophysical fluid problems, *Rev. Geophys.*, *20*, 851–875.

Merrifield, M. A., and P. E. Holloway (2002), Model estimates of M_2 internal tide energetics at the Hawaiian Ridge, *J. Geophys. Res.*, *107*(C8), 3179, doi:10.1029/2001JC000996.

Moore, A. M., H. G. Arango, E. Di Lorenzo, B. D. Cornuelle, A. J. Miller, and D. J. Neilson (2004), A comprehensive ocean prediction and analysis

system based on the tangent linear and adjoint of a regional ocean model, *Ocean Modell.*, *7*, 227–258.

Moore, A. M., H. G. Arango, E. Di Lorenzo, A. J. Miller, and B. D. Cornuelle (2009), An adjoint sensitivity analysis of the Southern California Current circulation and ecosystem, *J. Phys. Oceanogr.*, *39*, 702–720.

Munk, W. H. (1966), Abyssal recipes, *Deep Sea Res.*, *13*, 707–713.

Nash, J. D., M. H. Alford, and E. Kunze (2005), Estimating internal wave energy fluxes in the ocean, *J. Atmos. Oceanic Technol.*, *22*, 1551–1570.

Nash, J. D., E. Kunze, C. M. Lee, and T. B. Sanford (2006), Structure of the baroclinic tide generated at Kaena Ridge, Hawaii, *J. Phys. Oceanogr.*, *36*, 1123–1135.

Pinkel, R., and D. Rudnick (2006), Editorial, *J. Phys. Oceanogr.*, *36*, 965–966.

Rainville, L., T. M. S. Johnston, G. S. Carter, M. A. Merrifield, R. Pinkel, P. F. Worcester, and B. D. Dushaw (2010), Interference pattern and propagation of the M_2 internal tide south of the Hawaiian Ridge, *J. Phys. Oceanogr.*, *40*, 311–325.

Ray, R. D., and G. T. Mitchum (1996), Surface manifestation of internal tides generated near Hawaii, *Geophys. Res. Lett.*, *23*, 2101–2104.

Ray, R. D., and G. T. Mitchum (1997), Surface manifestation of internal tides in the deep ocean: Observations from altimetry and island gauges, *Prog. Oceanogr.*, *40*, 135–162.

Robertson, R. (2006), Modeling internal tides over Fieberling Guyot: Resolution, parameterization, performance, *Ocean Dyn.*, *56*, 430–444.

Rudnick, D. L., et al. (2003), From tides to mixing along the Hawaiian Ridge, *Science*, *301*, 355–357.

Shchepetkin, A. F., and J. C. McWilliams (2003), A method for computing horizontal pressure-gradient force in an oceanic model with a nonaligned vertical coordinate, *J. Geophys. Res.*, *108*(C3), 3090, doi:10.1029/2001JC001047.

Shchepetkin, A. F., and J. C. McWilliams (2005), The Regional Oceanic Modeling System: A split-explicit, free-surface, topography-following-coordinate ocean model, *Ocean Modell.*, *9*, 347–404.

Simmons, H. L., R. W. Hallberg, and B. K. Arbic (2004), Internal wave generation in a global baroclinic tide model, *Deep Sea Res., Part II*, *51*, 3043–3068.

Veneziani, M., C. A. Edwards, and A. M. Moore (2009), A central California coastal ocean modeling study: 2. Adjoint sensitivities to local and remote forcing mechanisms, *J. Geophys. Res.*, *114*, C04020, doi:10.1029/2008JC004775.

Zhang, W. G., J. L. Wilkin, J. C. Levin, and H. G. Arango (2009), An adjoint sensitivity study of buoyancy- and wind-driven circulation on the New Jersey Shelf, *J. Phys. Oceanogr.*, *39*, 1652–1668.

Zilberman, N. V., J. M. Becker, M. A. Merrifield, and G. S. Carter (2009), Model estimates of M_2 internal tide generation over Mid-Atlantic Ridge topography, *J. Phys. Oceanogr.*, *39*, 2635–2651.

Zilberman, N. V., M. M. Merrifield, G. S. Carter, D. S. Luther, M. D. Levine, and T. J. Boyd (2011), Incoherent nature of M_2 internal tides at the Hawaiian Ridge, *J. Phys. Oceanogr.*, *41*, 2021–2036.